ISSN: 2230-9926

Available online at http://www.journalijdr.com

IJDR

International Journal of Development Research
Vol. 10, Issue, 09, pp. 40722-40731, September, 2020
https://doi.org/10.37118/ijdr.19933.09.2020

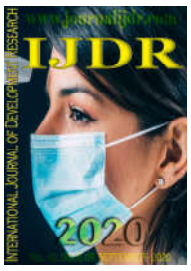

RESEARCH ARTICLE OPEN ACCESS

A DETERMINISTIC AND TUNABLE ALGORITHM FOR AUTOMATIC SWITCHOVER TO THE MOST SUITABLE RENEWABLE SOURCE ACCORDING TO POWER GENERATION

Alex de L. e Silva, *Geraldo M. Azevedo Jr, Vinicius C. de Oliveira, André F. A. M. Guimarães, Tallis A. Simões, Fabricio R. Neves, Paulo T. P. dos Santos and Octávio C. Ferrari

FOX PRIME Treinamento e Soluções em Energia, Rio de Janeiro – RJ, Brazil

ARTICLE INFO

Article History:
Received 17th June 2020
Received in revised form
28th July 2020
Accepted 16th August 2020
Published online 30th September 2020

Key Words:
Algorithmic decision-making; Deterministic algorithm; Tunable algorithm; Solar energy; Wind energy; Renewable energy; Substation auxiliary services; Operational technology; Embedded system.

Corresponding author:
Geraldo M. Azevedo Jr

ABSTRACT

This paper introduces a deterministic algorithm applied to the automatic switchover to the most suitable among two renewable power sources, namely photovoltaic and wind, aiming at achieving optimal usage of these supplies while respecting simplicity and affordability criteria. The approach to the algorithm's decision making is conventional logic based on power generation conditions. The proposed algorithm successfully copes with the bouncing problem that may occur when a choice based on simple comparison of the power values from the sources is adopted. Major parameters of the algorithm can be tuned, letting the operator perform optimizations according to local generation conditions and seasonal variations, favoring one power supply or the other. The realization of the algorithm is supported by novel hardware and software implementations. Although the algorithm was originally designed with the purpose of increasing reliability and availability of substations auxiliary services through the insertion of renewable power sources as alternative to the traditional supplies, it can be used in several other standalone applications. The simulation results presented in this piece of work, as well as the breadboard tests conducted, confirm the effective operation of the algorithm.

Citation: ***Alex de L. e Silva, Geraldo M. Azevedo Jr, Vinicius C. de Oliveira, André F. A. M. Guimarães, Tallis A. Simões, Fabricio R. Neves, Paulo T. P. dos Santos and Octávio C. Ferrari. 2020.*** "A Deterministic and Tunable Algorithm for Automatic Switchover to the Most Suitable Renewable Source According to Power Generation*", International Journal of Development Research*, 10, (09), 40722-40731.

INTRODUCTION

A hybrid, integrated solar photovoltaic (PV) and wind turbine (WT) based generation system can be an appealing solution for some specific standalone applications, such as auxiliary services of power substations. Power substations – pivotal elements to deliver electric power to the consumers, that is, to our houses, industries, shops, etc. – rely on the auxiliary services, which assure the proper conditions for the operation of the entire substation, e.g. supplying electricity at voltage levels suitable for the functioning of protection systems and control systems' equipment. According to ANEEL, the Brazilian Electricity Regulatory Agency, 1096 forced shutdowns occurred in the power transmission system in 2017 (ANEEL, 2018), partially due to problems in the substations auxiliary services. The significant number of failures in the substations auxiliary services and their impacts were the driving factors for proposing a system dedicated to increasing the reliability and availability of the substations auxiliary services through the insertion of PV and WT based power sources as alternative to the traditional supplies, such as mains power and diesel generator. Albeit solar and wind power are intermittent, they are temporally complementary (Giraud and Salameh, 2001; Naeem et al., 2019). By optimally combining these two renewable power sources, the impact of the variable nature of solar and wind resources can be partially resolved, yielding less costs, reduced energy storage size and better reliability (Al Badwawi, 2015). Our proposal is to connect the outputs from the PV and WT subsystems to battery banks, which, in turn, can service the loads in the substation either directly or through inverters. Eventually, the outputs can be straightforwardly connected to the existing common direct current (DC) bus of the substation auxiliary service. The most suitable renewable source according to the respective power generation conditions is to be automatically selected by the system as the active generator. The simplest approach to that would be switching over to the supply generating the greatest instantaneous power. However, this could result in bouncing

("ping pong" effect), especially when both systems instantaneous power values are very close. Bouncing can be troublesome and should be avoided, thus the algorithm must cope with it. Prior to the conception of the algorithm herein presented, some potentially applicable methods were evaluated. Literature brings similar yet non-identical architectures (Al Badwawi, 2015; Giraud and Salameh, 2001; Silva, 2014; Zhou et al., 2007). In (Harley and Liang, 2011), an overview on computational intelligence techniques for smart grids is provided. Clearly, decision-making algorithms based on fuzzy rules were natural prospects for our solution. Applications of fuzzy logic control that were reviewed include droop control for power sharing in wind and PV-based isolated microgrid (Kafle and Ni, 2016); frequency control of isolated wind and diesel hybrid microgrid (Marzband et al., 2011); optimal load sharing between multiple inverters connected in a smart house (Miyagi et al., 2013); and state-of-charge balance of distributed energy storage systems for DC microgrids (Diaz et al., 2014). Still, those works differ from ours in many ways, since they involve, either individually or in a combined fashion, droop control of inverters, state of charge monitoring of the batteries and frequency control of alternating current (AC) generators, which do not match the envisioned application of our proposed algorithm. One peculiarity of our proposed system is to aim at obtaining maximum efficiency from simple hardware and software, and fuzzy logic control would increase the complexity. Besides, no feedback to the generators or from the load/batteries is foreseen whatsoever.

In short, the purpose of this work is to study and apply algorithms and programming, supported by simple, dedicated electronics, to optimize the usage of renewable, environmentally-friendly power generation systems aiming at increasing the reliability of substation auxiliary services. The system being proposed can be categorized as an Operational Technology (OT) for it fits the definition of OT, i.e. "hardware and software that detects or causes a change, through the direct monitoring and/or control of industrial equipment, assets, processes and events" (Gartner, 2020). It can also be considered an Embedded System, since it is "a combination of computer hardware and software designed to perform a dedicated function" (Barr and Massa, 2006). The proposed system is based on novel hardware design and novel software implementation. Although the system performs in an autonomous manner, it provides a simple user interface to display some basic data and to allow the parameters setup. In the future, some sort of connectivity may be implemented with a few hardware and software modifications.

The development of the algorithm discussed in this article is part of an Research and Development (R&D) Project entitled "*Utilização e aplicação de um método determinístico adaptativo otimizado dedicado para o aumento da confiabilidade e disponibilidade do serviço auxiliar de subestações com a inserção de fonte solar fotovoltaica e eólica*" ("Utilization of a deterministic adaptable optimized method for reliability and availability increase of auxiliary services of substations with insertion of solar-photovoltaic and wind energy"), proposed and initiated by the concessionaires ODOYÁ TRANSMISSORA DE ENERGIA S.A., ESPERANZA TRANSMISSORA DE ENERGIA S.A. and TRANSMISSORA JOSE MARIA DE MACEDO DE ELETRICIDADE S.A in partnership with the executing company Fox Prime Treinamento e Soluçõesem Energia, adhering to the Act no. 9991/2000 (Brasil, 2000), ANEEL's R&D manual (ANEEL, 2012a), ANEEL Resolution no. 504/2012 (ANEEL, 2012b) and ANEEL Resolution no. 754/2016 (ANEEL, 2016) under Contract no. 38-CT-EC-134; 39-CT-EC-126; 41-CT-EC-036 FOX PRIME P&D.

MATERIALS AND METHODS

System overview: the integrated system architecture is depicted in Figure 1. In the present implementation, off-grid solar PV and wind generators are connected to the battery bank by charge controllers. The wind generator comprises the wind turbine, a built-in rectifier and the dump load (not shown in Figure 1). The instantaneous DC voltages and currents generated by the PV and WT subsystems are measured with appropriate sensors and circuitry, and input to the signal conditioning unit at the control system's panel. The core of the control system's panel is the control board, which contains the microcontroller (μC) that runs the algorithm. A DC/DC converter unit powers the boards at the control system's panel; this enhances the isolation. At the off-grid charge controllers' panel, there exists one contactor switch associated to each generation subsystem. These contactor switches, driven by the actuators at the control system's panel, open/close in order to cut off/allow the power from the respective subsystem to the battery bank according to the output of the algorithm.

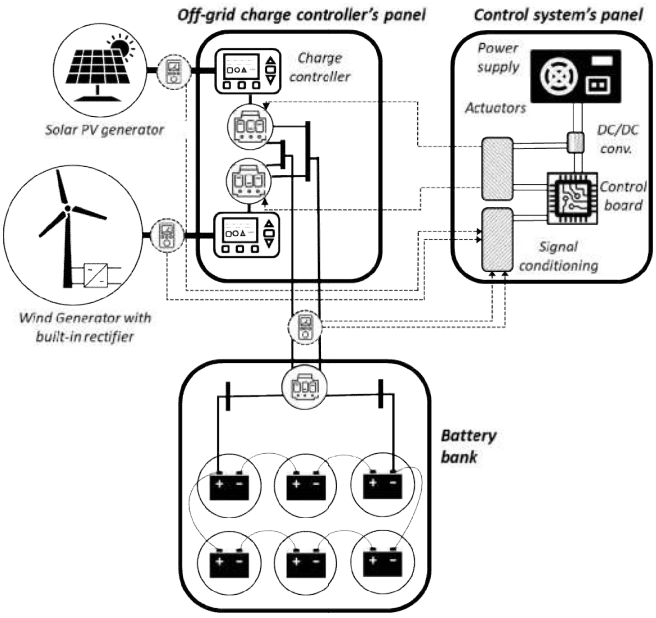

Figure 1. The proposed system architecture

Description of the Algorithm

The purpose of the algorithm is to decide and switch over to the most suitable among two (or more) sources, one at a time, according to power generation conditions. These power sources are intended to supply a battery bank and/or a critical load, as shown in Figure 2. From the conceptual standpoint, the output of the algorithm – henceforth referred to as *state* – corresponds to the position of a "virtual" selector switch. In this project, "State 1" means that the PV system has been temporarily selected as the active power supply, and "State 2" indicates that the WT based system is the provisionally choice as the active power supply. The algorithm also devises "State 0", where no source is selected. In case other sources are added, the algorithm could be scaled with minor modifications.

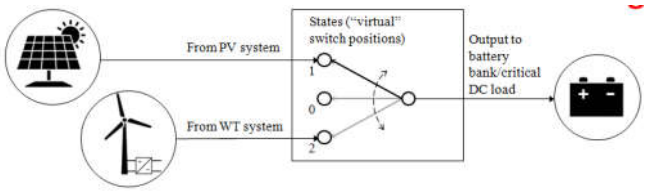

Figure 2. Conceptual representation of the algorithm as the "virtual" selector switch command

The main inputs to the algorithm are the values of instantaneous power generated by both systems. Let us name IPP and IPT the instantaneous powers from the PV and WT systems, respectively. Choosing the power source based on a simple comparison criterion may result in bouncing (especially when IPP and IPT values are close), which yields unnecessary switching in the short run and undesired consequences, e.g. wear of mechanical parts of contactor switches, electrical transients, etc. In order to avoid such phenomena, a power margin value is inserted. Figure 3. Presents the problem and Figure presents the proposed solution. A change of state can only occur when the concurrent system instantaneous power overcomes the active system instantaneous power plus the power margin value.

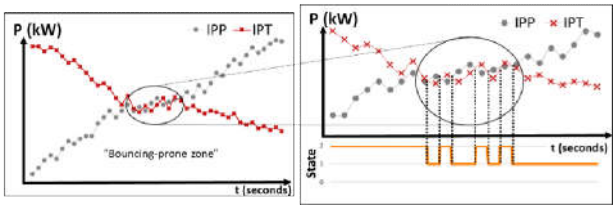

Figure 3. Switching over to the supply generating the greatest instantaneous power may result in bouncing when both power values are close

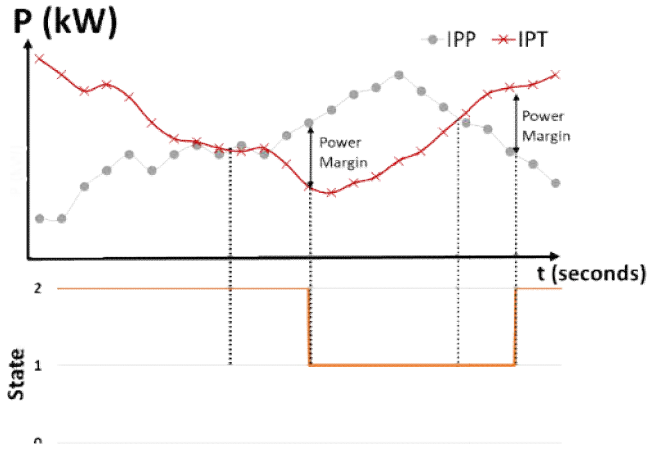

Figure 4. Adding a power margin avoids the bouncing problem. A change of state only occurs when the power margin is surpassed.

In the present implementation, the power margin is associated to the parameter called CHGMRG, which is operator-configurable. The decision logic can be more easily understood through a simple example in the form of pseudocode, as follows. Assuming that the active system is the PV system, i.e. the output variable OUTST holds the value "1":

OUTST = 1 *//current state value; 1 = PV, 2 = WT*
if IPP < (IPT − CHGMRG)
then OUTST = 2 *//new state value when the logical test above evaluates to true*

Comparably, when OUTST = 2 (meaning the active system is the WT system), IPT is evaluated against (IPP − CHGMRG). The algorithm computes IPP and IPT by applying a sliding window method. Figure illustrates the way this is performed. The instantaneous power generated by each system is sampled. The sample set size, i.e. the window length, is defined by the parameter called NSAMPLE. In the present implementation, NSAMPLE is an operator-configurable integer value ranging from 1 to 32. The IPP and IPT values to be utilized by the algorithm are actually the average over the number of samples taken, that is:

$$IPx = \left(\sum_{i=1}^{NSAMPLE} IPx\_SAMPLE_i \right) \Big/ (NSAMPLE)$$

where *x* denotes the system (*x* = P for the PV system, and *x* = T for the WT system). Let us review the example of Figure 5, where NSAMPLE = 4 and the PV system is considered. The first four samples compose the first set: {0.32, 0.31, 0.30, 0.30}, whose average is IPP, IPP = 0.3075 (in kW). Then, the window slides; the oldest sample (#1) is replaced with a new sample (#5) to constitute the second set: {0.31, 0.30, 0.30, 0.31}, which yields IPP = 0.3050 kW.

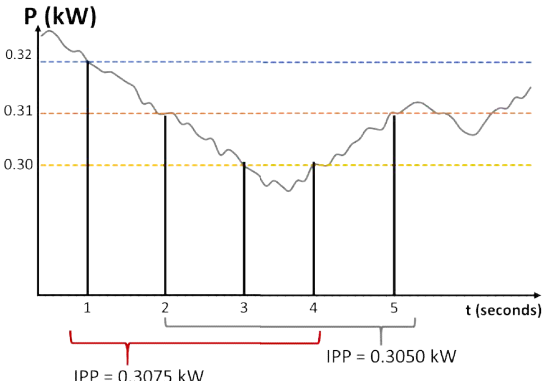

Figure 5. Averaging IPP using the sliding window method, NSAMPLE= 4.

Averaging the instantaneous power presents some advantages. Firstly, the algorithm benefits from a more stable value. Secondly, one single sample fortuitously missed (for instance, due to sensor read error) may not affect the overall result if NSAMPLE is large enough. As for the sampling period, it depends on the speed the code runs, which is subject to the clock of the circuit, delays deliberately inserted into the code, etc. The sampling period has no major influence as long as the systems are sampled at the same rate. An additional parameter to be considered by the algorithm is the minimum acceptable instantaneous power generated by the systems, defined by the MIN_IP parameter. When both systems' power is below MIN_IP, the output of the algorithm is "State 0". To avoid bouncing, the concept of power margin is here applied to the decision to enter/exit from "State 0". Still, a slight modification to the primary application of the CHGMRG parameter is necessary because MIN_IP involves values lower than the usual generation levels of the systems, that is, MIN_IP is typically much less than IPP and IPT. Therefore, the power margin for "State 0" transitions shall correspond to 10% of CHGMRG's configured value. In the present implementation, MIN_IP value is the same for both systems and can be

configured by the operator. Figure 6 exemplifies "State 0" to/from transitions. The transition to "State 0" can also be interpreted in the form of the following pseudocode:

if (IPP < (MIN_IP – CHGMRG/10)) and (IPT < (MIN_IP – CHGMRG/10))
then OUTST = 0

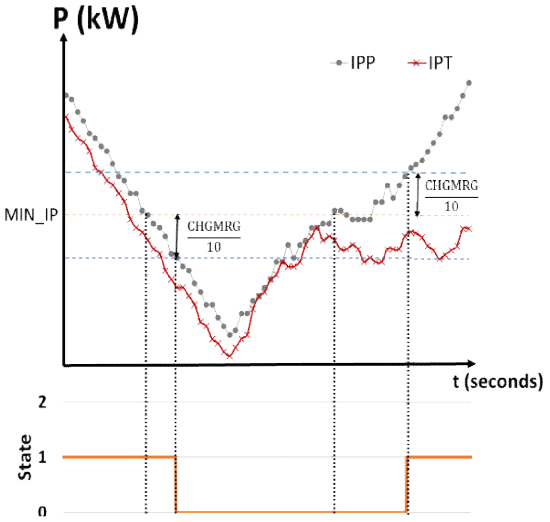

Figure 6. Operation of the MIN_IP parameter with downscaled power margin

The INB_TIME_P and INB_TIME_T parameters provide further enhancement regarding unwanted, frequent changes of state by setting inhibition time intervals. Within the inhibition time interval, changing to the previous state is forbidden. It works as follows: whenever a change of state occurs, an internal timer TIMER_T1 is restarted; while TIMER_T1 value is less than the inhibition time, the algorithm prevents changing back to the previous state. Let us examine Figure , which shows how these parameters affect the output of the algorithm (in this example, it is assumed that both IPP and IPT are greater than MIN_IP – otherwise, the output of the algorithm is "State 0"). At time t = t0, a change of state due to power occurs; the active power supply is now the WT system ("State 2"), and TIMER_T1 starts a new time count. Right after the change, IPT suddenly fades – for instance, due to a fleeting cloud. If only the power criterion was taken into consideration, this would lead to a momentary change to "State 1" (see the dotted red line on the bottom graph of Figure), and back to "State 2" as soon as the fleeting cloud is gone, i.e. IPT value normalizes. Such a situation is circumvented by applying a proper inhibition time, during which change of state is forbidden, regardless of the power criterion (see the solid blue line on the bottom graph of Figure for the corresponding output when the inhibition time is in effect). The INB_TIME_T parameter shown in Figure sets the inhibition time once a change to "State 2" occurs. INB_TIME_P acts similarly when a change to "State 1" occurs. Both parameters can be configured by the operator.

The example above can also be expressed in the form of the following pseudocode:

OUTST = 2 *//current state value: 2 = WT*
While TIMER_T1 < INB_TIME_T*//in case OUTST=1 // (PV), evaluate TIMER_T1 against INB_TIME_P*
OUTST = 2

end while

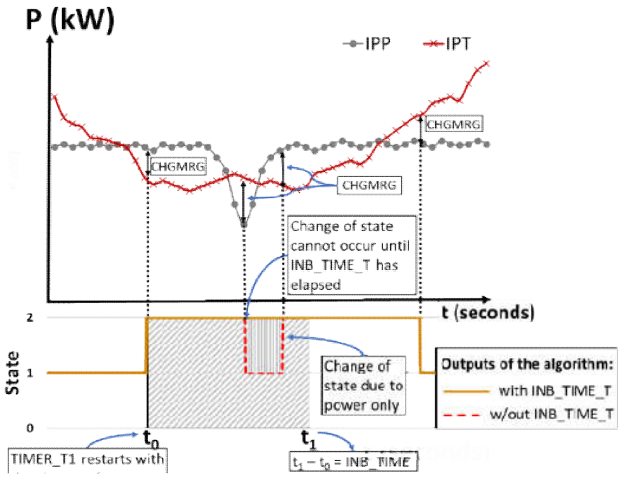

Figure 7. Application of the inhibition time parameter, INB_TIME_T

The parameter set of the current version of the algorithm is completed with PESO_P and PESO_T. These parameters define weights ("pesos", in Portuguese), and interact with CHGMRG. The higher the weight attributed to a certain system, the higher its priority. In practice, changing to that system is facilitated. Conversely, a lower weight value makes the change more difficult. The power margin is actually expressed as CHGMRG/PESO_*x*, where *x* denotes the concurrent system (*x* = *P* for the PV system, and *x* = *T* for the WT system). Figure illustrates how PESO_*x* and CHGMRG interact. Let CHGMRG be 100 W and PESO_T be 1; the power margin to be surpassed when switching to the WT system is 100 W/1 = 100 W. Let us also assume PESO_P = 2. By comparison, the power margin for switching to the PV system is lower in this case: 100 W/2 = 50 W. By setting the value of PESO_P to "2" instead of "1", the change to "State 1" is anticipated. On the other hand, in case PESO_P = 0.5, the power margin becomes 100 W/0.5 = 200 W and the change is delayed. PESO_P and PESO_T are operator-configurable. Table 1 summarizes the parameter set. User interface allows the adjustment within the described ranges at additive or multiplicative steps, depending on the parameter. Most of the default values were defined based on the authors' experience with solar PV and wind generators.

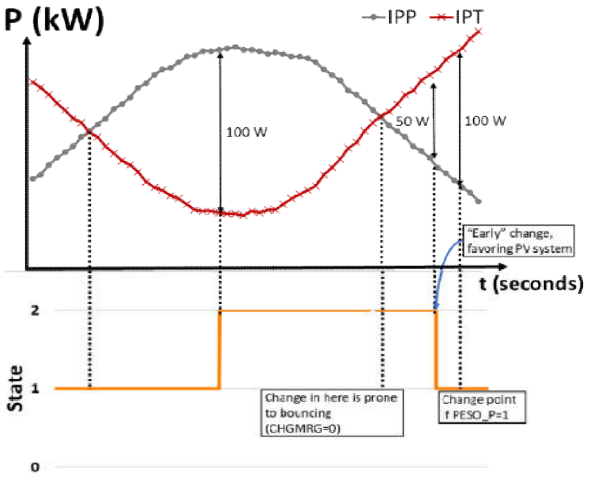

Figure 8. Change to "State 2" occurs at 100% of CHGMRG as the weight of WT (PESO_T) is 1; change to "State 1" occurs at 50%, since the weight of PV (PESO_P) is 2

Table 1. Tunable parameters, respective adjustment ranges and steps, default values and unit of measurement

Parameter	Range	Steps	Default value	Unit
CHGMRG	0 – 600	+50/-50	100	W
NSAMPLE	1 – 32	+1/-1	10	
MIN_IP	0 – 300	+5/-5	50	W
INB_TIME_P	0 – 300	+15/-15	60	s
INB_TIME_T	0 – 300	+15/15	300	s
PESO_P	0.5 – 2	×2/-2	1	
PESO_T	0.5 – 2	×2/-2	1	

NSAMPLE optimization: the default value of NSAMPLE was determined empirically, considering the four scenarios summarized in Table 2. On every case, CHGMRG was 100 W (default) and the instantaneous power of the concurrent system, IP_1, was arbitrarily fixed at 1900 W. Let us initially analyze "Scenario 1". In this scenario, the instantaneous power of the active generator, IP_2, is assumed to be 1700 W, and NSAMPLE = 20. Now, if one sample is missed in the measurement of IP_1, the averaged value of IP_1, i.e. IP'_1 is 1805 W. The difference between IP'_1 and IP_2 is still greater than CHGMRG, therefore the change of state can occur even if a single sample is misread. For two samples missed, however, IP'_1 would be 1710 W, yielding no change of state. In "Scenario 2", the active generator power is lower, IP_2 = 1600 W. Since the difference increases, the value of NSAMPLE that ensures correct operation can be reduced to 10 (IP'_1 = 1710 W with one read error and $|IP_2 - IP'_1|$ = 110 W, which is still greater than CHGMRG). Concisely, the smaller the power difference, the larger NSAMPLE has to be in order to make room for read error (as is the case of "Scenario 3"), and vice-versa ("Scenario 4"). CHGMRG also plays an important role in finding the optimal value of NSAMPLE: the smaller CHGMRG, the smaller NSAMPLE can be. As an exercise, if CHGMRG was set to 50 W, NSAMPLE in "Scenario 2" could be set to 8 instead of 10 and yet the system would be able to sustain one missed sample. Anyway, a 300 W difference such as in "Scenario 2" was deemed feasible, thus NSAMPLE = 10 was selected as the default. Obviously, adjustments can be done accordingly; for example, if the electromagnetic interference (EMI) in the surroundings is harsh and may cause more frequent errors, the NSAMPLE value can be incremented.

Table 2. Scenarios considered for the definition of NSAMPLE default value

Scenario	NSAMPLE	IP'_1 (W)	IP_2 (in W)	$\|IP_2 - IP'_1\| >$ CHGMRG?
1	20	1805,00	1700	Yes
2	10	1710,00	1600	Yes
3	32	1840,63	1740	Yes
4	4	1425,00	1300	Yes

Implementation considerations: the algorithm can be implemented in many ways, according to the customer's taste, but we opted for PIC µC for our design. The program – including the algorithm core features, input/output interfacing and fault signaling functions – was written in high-level language (C language) and compiled with MPLAB® X IDE v. 5.25 (Microchip, 2019a) using the MPLAB® XC8 compiler, v. 2.10 (Microchip, 2019b). The current version of the program uses 37.800 B, which makes the PIC18F4685 model a suitable choice, as its program memory size is 96 kB (Microchip, 2007).

Because both generation systems supply DC power, the power measurement circuitry is greatly simplified. To measure current, Hall-effect transducers are employed. The signal produced by each current transducer is applied to an analog-to-digital (A/D) input of the µC, and the program performs the operations to calculate the effective corresponding current I, in amperes, for each current sample. To measure the voltage generated by each system, separate voltage dividers and conditioning circuits based on operational amplifiers are utilized to reduce the DC voltage to values proper for application to the A/D inputs. Likewise, the program performs the necessary operations to compute the actual voltage V, in volts, for each voltage sample. $V \times I$ results in a sampled instantaneous power value which composes the calculation of IPP or IPT together with NSAMPLE. Two digital outputs of the µC are utilized to represent the states (binary "01" and binary "10"). The contactor switches that connect/disconnect the power supplies to/from the battery bank can be indirectly driven by these outputs by some sort of photocoupling.

Fault signaling: failure signaling of the current and voltage sensors is foreseen by the system. For clearer understanding, let us resort to Figure ; in this illustration, the power generated by the WT system is being measured while the active system is the PV system. The DC voltage V produced by the wind generator is downscaled by the voltage divider composed of the resistors R_1 and R_2 and the corresponding signal is applied to the input of the control board. R_1 and R_2 values should be high so that the current I_2 through them is negligible in relation to the total DC current I yielded by the WT system. I is measured with the aid of a Hall-effect transducer; the proportional voltage signal is handed over to the control system's panel for the required calculations. Since the WT system is the concurrent one – hence, momentarily disconnected from the batteries/effective DC loads –, a dummy load of low ohmic value is required in order to let the current continue flowing under this circumstance. In case the PV system is the concurrent one, the same scheme applies.

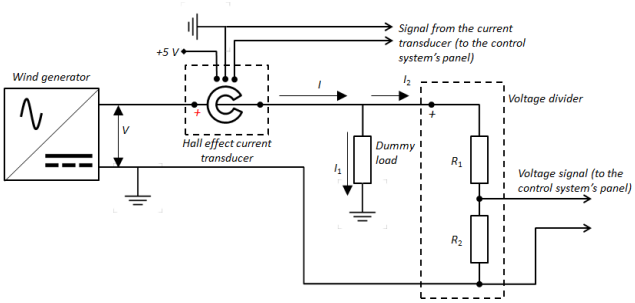

Figure 9. Scheme to measure the power from the WT system

EMI can negatively affect Hall effect current sensors by inducing phantom currents. For this reason, the program code defines, via the NOISE_HALL parameter (non-changeable), a range around zero within which the current values can be considered as noise. Range boundaries correspond to +(NOISE_HALL) and –(NOISE_HALL). Sensor is inverted if the current I measured by it is less than –(NOISE_HALL). The code also sets a range to accommodate small positive variations in the DC voltage measurement part which can be regarded as noise due to quantization error in the A/D conversion. The upper boundary of this range is determined by the NOISE_VOLTAGE parameter (non-changeable), and the lower boundary is zero.

In normal operation, voltage and current are simultaneously high or low. In case of sensor failure, two cases can occur: if $I \geq$ +(NOISE_HALL) and $V <$ NOISE_VOLTAGE, i.e. high current and low voltage, either the voltage divider has been disconnected or one of the resistors is open; if $V \geq$ NOISE_VOLTAGE and –(NOISE_HALL) $< I <$ +(NOISE_HALL), i.e. high voltage and current about zero, it denotes damaged dummy load or current transducer. The program also handles inverted current sensor alarm: current must be input to the "+" terminal of the transducer, otherwise the measurement results disarray.

Simulation& prototyping: the algorithm operation was simulated using Proteus 8 Professional Release 8.4 SP0 Build 21079 with Advanced Simulation (Labcenter, 2020). The program in hexadecimal file format was loaded to the simulated µC. To simulate and vary the current and voltage signals utilized for power measurement, 5 V batteries and potentiometers were employed. LEDs were connected to the proper output pins for visual indication of the states. An extra LED was inserted only for debugging the inhibition time feature. LCD display, front panel buttons for menu navigation and real-time clock via I2C protocol were also simulated. The algorithm worked smoothly, as evidenced by the simulations and results discussed in the next section of this paper. Besides, the same hardware and software that were simulated in Proteus were implemented on breadboard. Results were identical to those obtained in the simulations. The hardware implementation itself shall be thoroughly discussed in a future work, including the assembling on the field with the connections to the PV panels and the wind generator.

RESULTS

First, let us consider the situation shown in Figure . IPP, was 1714 W (Pp indication on the display); IPT, was 623 W (Pt indication); and the parameters were set to their default values (in accordance with Table 1). Consequently, LED D1 was on and LED D2 was off, meaning the active system was the PV system ("State 1"). Since CHGMRG = 100 W and PESO_P = PESO_T = 1, the output could only change to "State 2" if IPT exceeded 1814 W (IPP value remaining fixed), as it can be verified in Figure . In this example, although IPT was greater than IPP (1767 W *vs*. 1714 W), the 100 W power margin prevented changing to "State 2", as indicated by D1 and D2. In Figure, the IPT value of 1852 W was high enough to surpass (IPP + CHGMRG). D1 turned off and D2 turned on, indicating the switch to the WT system ("State 2").

In the second simulation, PESO_P was set to 2; thus, the power margin for changing from "State 2" to "State 1" was 100 W/2 = 50 W, i.e. change of state could only occur if IPT dropped below 1664 W (IPP value remaining fixed). In Figure , IPT was less than IPP but still greater than 1664 W, hence the state remained the same. In Figure , IPT value of 1656 W was low enough to let the output change (D1 "on" and D2 "off"). Subsequently, PESO_T was set to 0.5. In this way, the power margin for changing from "State 1" to "State 2" was 200 W. The output could only change if IPT surpassed 1914 W (IPP value remaining fixed), which was not the case in Figure 5. Even though IPT > (IPP + CHGMRG), the lower weight attributed to the WT system prevented changing to "State 2", as indicated by D1 and D2. In Figure 16, however, the conditions for change were met.

The third simulation checks the working of MIN_IP parameter, whose value was initially set to 50 W. As the reduced power margin corresponding to 10% of CHGMRG is applied to changes to/from "State 0", both IPP and IPT must be less than 40 W to enter "State 0". In the simulation depicted in Figure 17, only the WT system was in very low power condition. IPP was slightly above 40 W; hence, the output was "State 1". Further reduction of IPP led to the change to "State 0" shown in Figure 18. Note that it must be assumed that the inhibition time has elapsed.

For demonstration of INB_TIME_P, the output pin RD1 of the µC was enabled by software so that LED D3 could remain "on" until the inhibition time had elapsed. For example, in Figure , the output of the system had just changed to "State 1" (D1 "on"); INB_TIME_P = 30 s. While the 30 s interval had not elapsed, D3 continued to be on and a change of state was denied regardless of the power conditions. This can be verified in Figure : the WT system outpowered the PV system; nevertheless, the algorithm held "State 1" due to the time restriction imposed. After the 30 s period, the change of state finally occurred, as depicted in Figure 21 (D2 "on", D1 "off"). It should be noted in Figure 21 that the power values were the same as in Figure , but the inhibition time of 30 s had expired (shown by D3 "off" and the clock on the display).

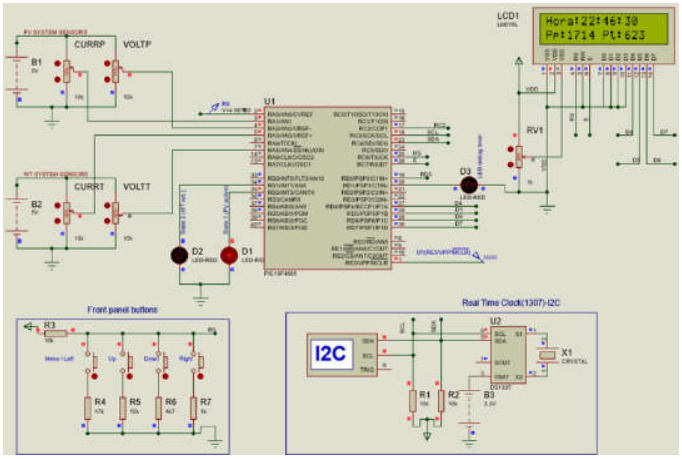

Figure 10. PV system produced the greatest power (1714 W), therefore it was the active one, as indicated by the LEDs (D1 "on" and D2 "off")

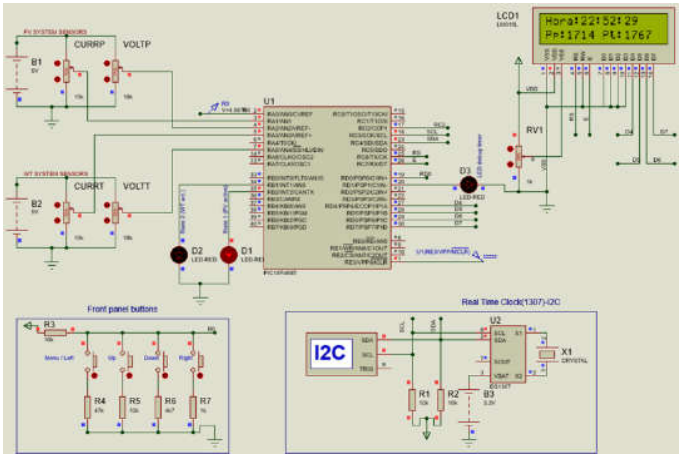

Figure 11. IPT was greater than IPP, but not greater than (IPP + CHGMRG); hence, the PV system remained as the active one

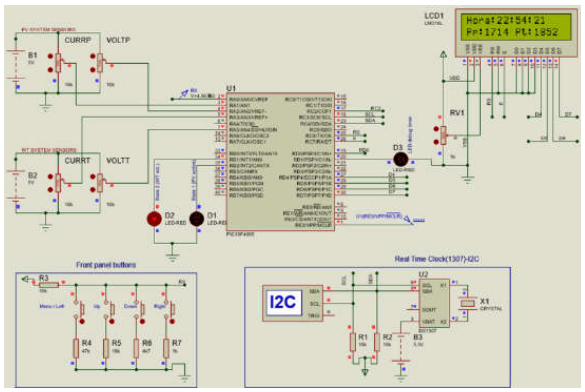

Figure 12. IPT was great enough to overcome (IPP + CHGMRG), yielding a change to "State 2".

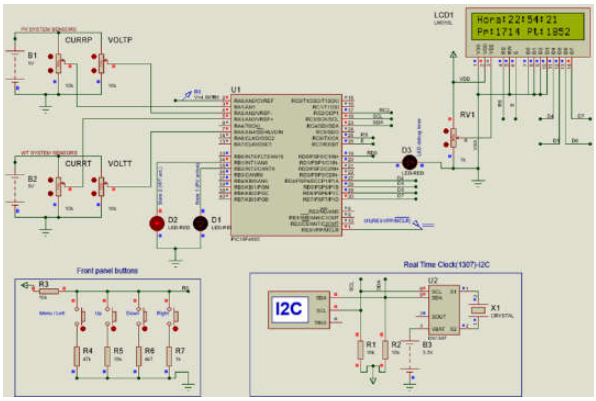

Figure 13. while output was "State 2", IPT dropped to less than IPP, but still within the power margin of 50 W (CHGMRG/2); no change occurred

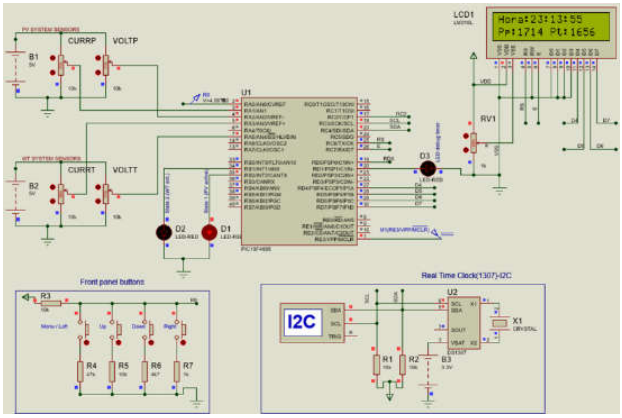

Figure 14: IPT dropped below [IPP – (CHGMRG/2)]; output changed to "State 1" as indicated by the LEDs

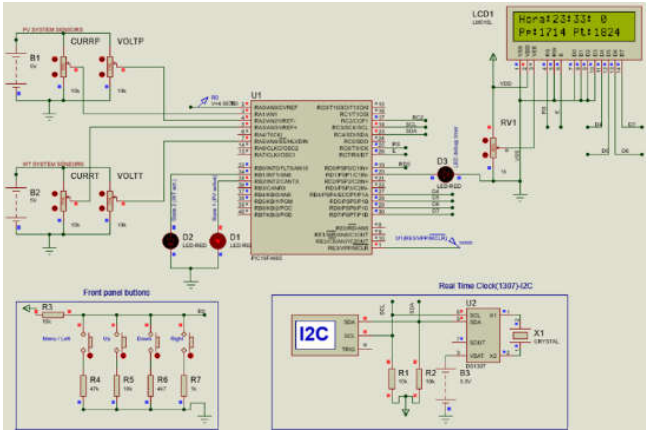

Figure 15: while output was "State 1", IPT exceeded IPP by more than CHGMRG, but no change to "State 2" occurred because PESO_T = 0.5

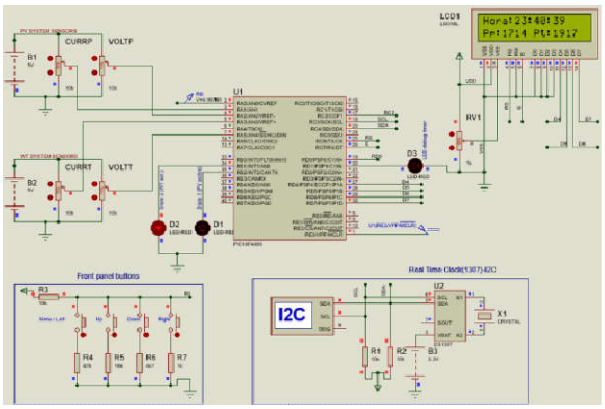

Figure 16. IPT was greater than {[IPP + (CHGMRG/0.5)] = 1914 W}, thus the output changed to "State 2" as indicated by the LEDs

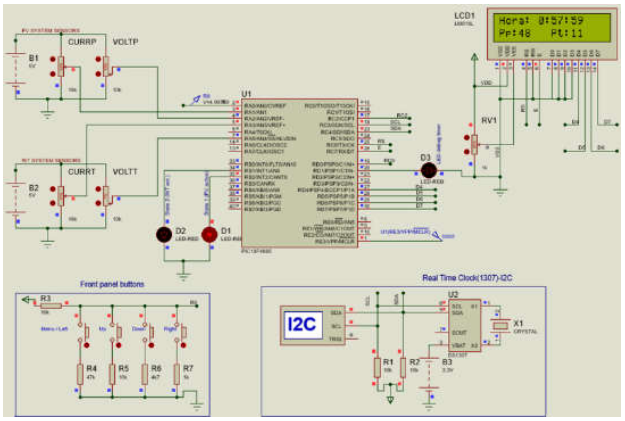

Figure 17: output was "State 1" for only WT system is in very low power condition, i.e. less than [MIN_IP - (0.1×CHGMRG)]

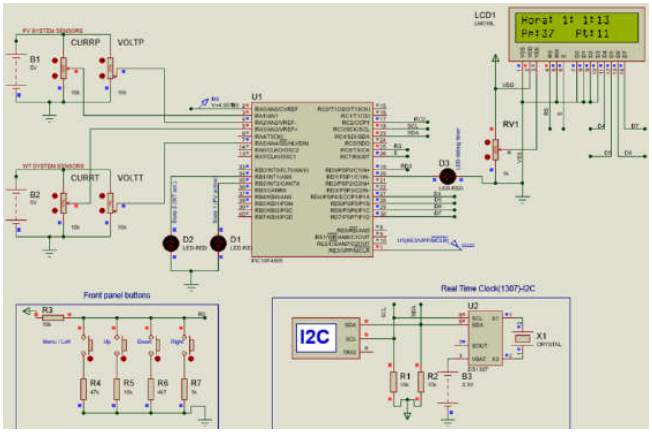

Figure 18. Output was "State 0" because both generation systems are in very low power condition (D1 and D2 "off")

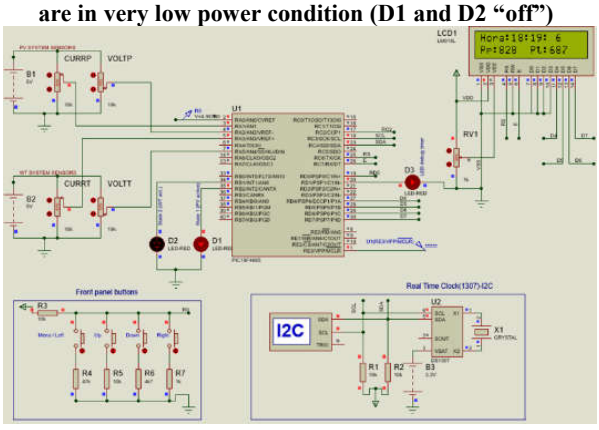

Figure 19. Output had just changed to "State 1" (D1 "on", D2 "off"); IPP was greater than IPT, and INB_TIME_P had not elapsed (D3 "on")

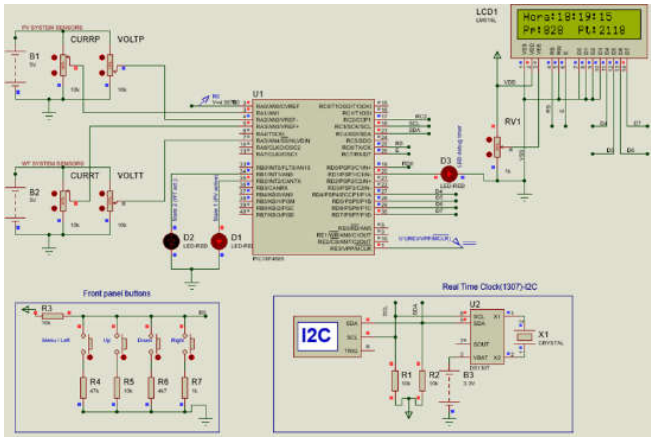

Figure 20. IPT of 2118 W greater than (IPP + CHGMRG), but no change of state occurred because INB_TIME_P had not elapsed (D3 still "on")

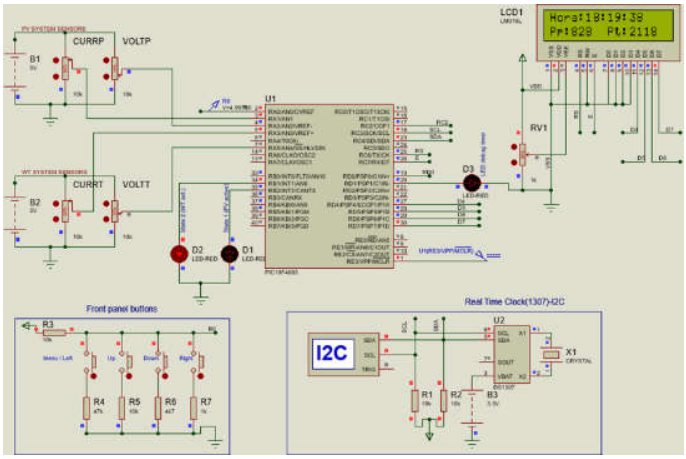

Figure 21. Same power conditions as the previous figure; INB_TIME_P had elapsed (D3 "off"), and output could change to "State 2" (D1 "off", D2 "on")

DISCUSSION

The proposed algorithm switches over to the most suitable source subject to the power generation conditions and the defined parameterization. Such approach – that is, selecting the best among two (or many) power supplies – aims at tackling the main challenge for standalone systems, which is the high storage cost, for it implies leaner-sized, cheaper storage. This is particularly interesting in the case of a hybrid photovoltaic and wind system because of the inherent temporal complementarity of such energy sources. The search for simplicity and affordability that guided the development of the proposed system is, therefore, met. The most elementary approach to power-based source selection would be to perform the simple comparison between the output values of the generation systems. However, this approach is prone to bouncing when the output values are too close. Bouncing should be avoided by all means because it implies needless switching. The proposed algorithm was intended to solve, through its parameters, the bouncing issue. The key to achieving this goal was the introduction of a power margin parameter in such a way that a change of state can only happen when the concurrent system instantaneous power exceeds the active system instantaneous power plus the power margin value. The algorithm also resorts to time inhibition parameters; immediately after a change of state, a time interval during which changing back to the previous state cannot occur is set, regardless of the power criterion. This serves to accommodating relatively fast variations on the wind speed or the insolation. The proposed system is designed to enable scalability, robustness and flexibility with relatively low complexity modifications. Regarding scalability, additional power supplies can be implemented by simple changes in the software. Expansion is limited by hardware, i.e. the amount of input/output ports available. Generation systems which require power measurement need two analog input ports. Power measurement-free generation systems, such as emergency diesel generators, are exempt from this requirement. On the output side, each power supply demands one digital port. The number of output ports can be further increased if an n-to-2^n decoding scheme with integrated circuit is adopted.

Robustness is accomplished through a combination of software and hardware techniques. In the software domain, processing multiple power samples to obtain an average value, as implemented by design, can compensate for transient read errors if the number of samples taken – which is a tunable parameter of the algorithm – is large enough. The program also features sensors health check routines and failure alarms to assist in corrective maintenance. Hardware robustness level depends on the application requirements. For instance, in a power substation environment, EMI effects can be mitigated through the use of a DC/DC converter to electrically isolate the control system's boards from the mains. Proper shielding of the control system's panel/boards is strongly advisable, too. Further fault tolerance can be achieved with hardware redundancy. In this sense, a secondary control board may be included, either operating on standby or on a round robin scheme. Setting up redundant current/voltage sensing circuits is also an alternative. From the perspective of system flexibility, one aspect to be considered is whether the generation type is DC or AC (or mixed). The generators employed in the present implementation supply DC power – the photovoltaic panels are intrinsically DC, and the wind turbine embodies a rectifier. This simplifies the power calculation to a great extent. Should AC power be involved instead, proper techniques for computing apparent power must take place. Another attribute to be looked upon is whether the power sources feed the loads directly or are used to charge battery banks. In the latter scenario, which is the current implementation, a short disconnection time during changes of state is tolerable. In the first situation, however, voltage sags during state transitions may be unacceptable; as a countermeasure, short hold times before disconnection of the previously active system can be introduced, which is ordinary to realize by software.

The system grants the operator freedom to perform adjustments according to season characteristics. The parameters can be tuned to favor one generation system or the other depending on the average wind speed and insolation at the installation site. To this end, distinct weights can be assigned to the generation systems based on the knowledge of local conditions. Different values of power margin and inhibition times may also be experimented. Although the proposed system contemplates substation auxiliary services, it can be applied to any standalone application. It is worth emphasizing that the proposed system particularly benefits from the complementarity of photovoltaic and wind sources. Owing to this fact, the location of Juazeiro III in the state of Bahia – Brazil was defined as a convenient option for installation given its natural characteristics (such inference is

well documented in the reports of the early stages of this R&D project). Therefore, the next step is to perform on-site tests. The simulations and breadboard tests corroborated the smooth working of the algorithm, which behaved just as expected – in other words, the system is fully prepared for the field tests –, but the generation conditions for both PV and WT systems in our laboratory, located in the city of Rio de Janeiro, were not favorable, thus hindering further testing. The proposed control system allows for possible future improvements. Connectivity may be implemented with minor hardware and software modifications. RS-485/RS-422 serial interfacing with the μC can be accomplished with an adequate transceiver, such as the MAX3140 (Maxim, 2010). Once communication capabilities are available, data can be exported to a computer for statistical analysis, for instance. An even more promising feature is the communication with power electronic equipment, such as inverters. Depending on what information these devices are able to provide – for example, output frequency –, additional parameters can be obtained to support not only power-based source selection but also quality-based source selection. Additionally, if differentiated tariffs according to the hour apply to the client, some sort of time-based optimization may be realized, since the system incorporates a real-time clock.

CONCLUSION

This paper presented a deterministic algorithm applied to the automatic switchover to the most suitable among two (or more) power sources, one at a time. On account of simplicity, the algorithm adopts conventional logic for its decision making, which is based on power generation conditions. A most elementary algorithm based on simple comparison criterion might let bouncing occur when both systems' output power values are too close, whereas the proposed algorithm copes with it by adding power margins and inhibition times. Core parameters of the algorithm are tunable, allowing the system operator to perform optimizations according to the power generation conditions at the site, e.g. wind speed and insolation, which vary seasonally. The results obtained from the simulations and the breadboard tests showed that the algorithm behaved exactly as devised, that is, it is ready for field tests.

Acknowledgment

The authors wish to thank the concessionaires ODOYÁ TRANSMISSORA DE ENERGIA S.A., ESPERANZA TRANSMISSORA DE ENERGIA S.A. and TRANSMISSORA JOSE MARIA DE MACEDO DE ELETRICIDADE S.A. for proposing and funding the present work in the form of an R&D Project (P&D – ANEEL) and to Universidade Santa Úrsula for the key contributions.

REFERENCES

Al Badwawi, R., Abusara, M., Mallick, T. A. 2015. Review of Hybrid Solar PV and Wind Energy System. Smart Science, vol. 3, no. 3.

Aneel 2012. Manual do programa de pesquisa e desenvolvimento tecnológico do setor de energia elétrica. Brasília, DF, Brazil: Agência Nacional de Energia Elétrica, 2012a In Portuguese.

Aneel 2018. Relatório de Análise: desligamentos forçados do Sistema de Transmissão. Brasília, DF, Brazil: Agência Nacional de Energia Elétrica In Portuguese.

ANEEL 2012. Resolução Normativa nº 504, de 14 de agosto de 2012 – Altera a Resolução Normativa n° 316, de 13 de maio de 2008. Brasília, DF, Brazil: Agência Nacional de Energia Elétrica, 2012b In Portuguese.

ANEEL 2016. Resolução Normativa nº 754, de 13 de dezembro de 2016 – Aprova os Procedimentos do Programa de Pesquisa e Desenvolvimento – PROP&D e altera os Submódulos 2.7: Outras Receitas e 9.1: Revisão Periódica das Receitas das Concessionárias Existentes dos Procedimentos de Regulação Tarifária – PRORET. Brasília, DF, Brazil: Agência Nacional de Energia Elétrica, 2016 In Portuguese.

Barr, M., Massa, A. 2006. Programming Embedded Systems: With C and GNU Development Tools. Sebastopol, CA, USA: O'Reilly Media Inc., 2nd edition.

Brasil 2000. Lei nº 9.991, de 24 de julho de 2000 – Dispõe sobre realização de investimentos em pesquisa e desenvolvimento e em eficiência energética por parte das empresas concessionárias, permissionárias e autorizadas do setor de energia elétrica, e dá outras providências. Brasília, DF, Brazil: Presidência da República In Portuguese.

Diaz, N. L., Dragičević, T., Vasquez, J. C., Guerrero, J. M. 2014. Fuzzy-Logic-Based Gain-Scheduling Control for State-Of-Charge Balance of Distributed Energy Storage Systems for DC Microgrids. Fort Worth, TX, USA: IEEE Applied Power Electronics Conference and Exposition – APEC 2014, pp. 2171-2176.

Gartner 2020. Gartner Glossary – Operational Technology OT. Stamford, CT, USA: Gartner Inc. Retrieved from https://www.gartner.com/en/information-technology/glossary/operational-technology-ot.

Giraud, F., Salameh, Z. M. 2001 Steady-State Performance of a Grid-Connected Rooftop Hybrid Wind-Photovoltaic Power System with Battery Storage. IEEE Transactions on Energy Conversion, vol. 16, no. 1.

Harley, R. G., Liang, J. 2011. Computational Intelligence in Smart Grids. Paris, France: 2011 IEEE Symposium Series on Computational Intelligence SSCI 2011, pp. 11–15.

Jiang, Z., Yu, X. 2008. Hybrid DC- and AC-Linked Microgrids: Towards Integration of Distributed Energy Resources. Atlanta, GA, USA: IEEE Energy 2030 Conference.

Kafle, L., Ni, Z. 2016. Fuzzy Logic Adjustment for Power Sharing in Wind and PV-based Isolated Microgrid. Athens, Greece: 2016 IEEE Symposium Series on Computational Intelligence SSCI 2016, pp. 136–142.

Labcenter 2020. PCB Design and Circuit Simulator Software – Proteus. England: Labcenter Electronics. Retrieved from https://www.labcenter.com/.

Marzband, M., Sumper, A., Gomis-Bellmunt, O., Pezzini, P., Chindris, M. 2011. Frequency Control of Isolated Wind and Diesel Hybrid Microgrid Power System by Using Fuzzy Logic Controllers and PID Controllers. Lisbon, Portugal: 11th International Conference on Electrical Power Quality and Utilisation EPQU 2011, pp. 130–135.

Maxim 2010. SPI/MICROWIRE-Compatible UART with Integrated True Fail-Safe RS-485/RS-422 Transceivers Datasheet. Sunnyvale, CA, USA: Maxim Integrated Products.

Microchip 2019. MPLAB® X Integrated Development Environment IDE. Chandler, AZ, USA: Microchip Technology Inc., 2019a. Retrieved from https://www.microchip.com/mplab/mplab-x-ide.

Microchip 2019. MPLAB® XC Compilers. Chandler, AZ, USA: Microchip Technology Inc., 2019b. Retrieved from https://www.microchip.com/mplab/compilers.

Microchip 2007. PIC18F2682/2685/4682/4685 Data Sheet. Chandler, AZ, USA: Microchip Technology Inc.

Miyagi, M., Morinaga, S., Shiroma, Y., Funabashi, T. 2013. Optimal Load Sharing using Droop Control and Fuzzy Control in Uninterruptible Smart House. Tainan, Taiwan: 2013 1st International Future Energy Electronics Conference IFEEC, pp. 103–108.

Naeem, A., Ul Hassan, N., Yuen, C., Muyeen, S.M. 2019. Maximizing the Economic Benefits of a Grid-Tied Microgrid Using Solar-Wind Complementarity. Energies 2019, 12, 395.

Silva, A. L. 2014. Protótipo de um sistema fotovoltaico auxiliar com armazenamento de energia elétrica. Masters dissertation in Technology Development. Curitiba, PR, Brazil: Instituto de Tecnologia para o Desenvolvimento – LACTEC In Portuguese.

Zhou, D., Jiang, Z., Li, Y., Fan, Q. 2007. A Small Grid-Connected PV System Controlled by the PLC. Proceedings of ISES World Congress, Vol. I - Vol. V, pp. 1528-1532.

****